Heliyon 10 (2024) e32335

Contents lists available at ScienceDirect

Heliyon

journal homepage: www.cell.com/heliyon

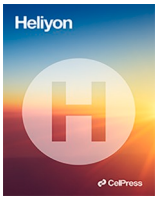

Research article

Comparative metabolomics analysis of *Citrus medica* var. sarcodactylis Swingle and *Limonia acidissima* Linn. Fruits and leaves cultivated in Egypt in context to their antiviral effects

Abeer M. El Sayed [a,*], Eman A.W. El-Abd [b], Ahmed H. Afifi [b], Fatma A. Hashim [b], Omnia Kutkat [c], Mohamed A. Ali [c], Mohamed A. El Raey [d], Seham S. El Hawary [a]

[a] *Pharmacognosy Department, Faculty of Pharmacy, Cairo University, Kasr El Aini Street, Cairo, 11562, Egypt*
[b] *Department of Pharmacognosy, National Research Centre, 33-Elbohouth St, (Former El-Tahrir St.), Dokki, P.O.12622, Giza, ID: 60014618, Egypt*
[c] *Center of Scientific Excellence for Influenza Viruses, National Research Centre, Dokki, 12311, Cairo, Egypt*
[d] *Department of Phytochemistry and Plant Systematics, Pharmaceutical Division, National Research Centre, Dokki, Cairo, Egypt*

ARTICLE INFO

Keywords:
UPLC-MS
Citrus medica
Limonia acidissima
Antiviral (H5N1)
Nano formulation
Docking

ABSTRACT

A comprehensive study of fruits and leaves extracts of *Citrus medica* var. *sarcodactylis* Swingle and *Limonia acidissima* L. family Rutaceae was accomplished to investigate their antiviral activity along with their zinc oxide nanoparticles formulation (ZnONPs) against the avian influenza H5N1 virus. A thorough comparative phytochemical investigation of *C. medica* and *L.acidissima* leaves and fruits was performed using UPLC-QTOF–MS-MS. Antiviral effects further aided by molecular docking proved the highly significant potential of using *C. medica* and *L.acidissima* extracts as medicinal agents. Antiviral potency is ascendingly arranged as *L. acidissima* leaves (LAL) > *L. acidissima* fruits (LAF) > *C. medica* leaves (CML) at 160 μg. Nano formulation of LAF has the most splendid antiviral upshot. The metabolomic profiling of CMF and LAL revealed the detection of 48 & 74 chromatographic peaks respectively. Docking simulation against five essential proteins in survival and replication of the influenza virus revealed that flavonoid di-glycosides (hesperidin, kaempferol-3-*O*-rutinoside, and kaempferol-7-neohesperidoside) have shown great affinity toward the five investigated proteins and achieved docking scores which approached or even exceeded that achieved by the native ligands. Hesperidin has demonstrated the best binding affinity toward neuraminidase (NA), haemagglutinin (HA), and polymerase protein PB2 (−10.675, −8.131, and −10.046 kcal/mol respectively. We propose using prepared crude methanol extracts of both plants as an antiviral agent.

1. Introduction

Respective new antiviral mediators are currently under development that might be efficient against the influenza virus, mostly the H5N1 avian flu virus. Derived plant extracts are the emphasis of several investigation due to their recognized useful healthiness effects in several disease problems [1]. Antiviral effects of several herbs were previously discussed [2] against viruses concerning, the effects in the host, and the claim methods the mode of action for emphasis on viral replication stages.

* Corresponding author. Pharmacognosy Department, Faculty of Pharmacy, Cairo University, Cairo 11562, Egypt.
E-mail address: abeer.ali@pharma.cu.edu.eg (A.M. El Sayed).

https://doi.org/10.1016/j.heliyon.2024.e32335
Received 2 August 2023; Received in revised form 30 May 2024; Accepted 2 June 2024
Available online 3 June 2024

Citrus medica var. *sarcodactylis* Swingle and *Limonia acidissima* L. are members of the *Rutaceae* family, which includes adherents of significant commercial value the most notable are *Citrus* species. According to a prior study, *C. medica* peel essential oils contain potent antiviral and antibacterial properties [3]. Triterpenoids, steroids, coumarins, *p*-coumaric acids, limonin, nomilin, etc. were all part of *C. medica.* In the peel oil from the Japanese fingered citron the major volatile components were limonene and γ-terpinene [4].

The only species in this genus is *Limonia acidissima* L. (syn. *Feronia elephantum*, *Feronia limonia* L.), which is commonly known as a wood apple. *L. acidissima* has phytochemicals phenolic such as coumarins, lignans, flavonoids, phenolic acids, and quinones, in addition to, triterpenoids, alkaloids, sterols, and volatile oils. Wood apples are reported to have anticancer, antioxidant, antidiabetic, hepatoprotective, antimicrobial, and larvicidal potentials [3,5]. At 200 g/ml, *L. acidissima* leaves ethanolic extract showed notable antibacterial activity comparable to that of ciprofloxacin [6,7]. Fruit extracts and the main bioactive ingredients as a source of antimicrobial candidates were recently studied [8]. Few studies were described to explore the antiviral effect of *C. medica* and *L. acidissima* [6–8]. To the finest of my information, this is the primary statement for the antiviral activity and metabolite profiles of both plants under investigation and their nano formulation. Our aims to identify phytoconstituents derived from *L. acidissima* and *C. medica* plants cultivated in Egypt by use of advanced spectroscopic and chromatographic techniques, in conjunction with antiviral screening. A docking study was carried out to decipher the mechanism and the secondary metabolites to which the antiviral activity was attributed. Furthermore, the impact of nano formulation on the biological activities of *C. medica* leaves (CML), *L. acidissima* leaves (LAL), and *L. acidissima* fruits (LAF) was evaluated. In the pharmaceutical sector, our goal is to develop efficient therapeutic agents derived from botanical sources.

2. Material & methods

2.1. Material for phytochemical studies

2.1.1. Plant material

Citrus medica var. *sarcodactylis* Swingle fresh fruits and leaves were collected from Mareii farm Gamgara, Banha, Qalyuobia https://goo. gl/maps/PKForD5kGcmLaDgh7. While *Limonia acidissima* L. fresh fruits and leaves were collected from Zoo Garden Giza https://goo.gl/maps/m87JstQpN1efnteM9 in March 2016 and verifier specimens were kept back at the department of pharmacognosy, faculty of pharmacy, Cairo University https://goo.gl/maps/v6PsvJp6KJW52PkH8 under no.29-12-2016 I & II. The specimens were identified by Mrs. Theresa Labib, consultant of taxonomy at the Ministry of Agriculture and the former director of El-Orman Botanical Garden https://goo.gl/maps/oeuQ2LTUbJmzMcap8.

Two kg of fresh *C. medica* and *L. acidissima* fruits and leaves were allowed to air dry for two weeks. Plant pieces were ground by impact and cutting size reduction method using an electric ultra-centrifugal mill ZM 200 (Retsch, Haan, Germany) equipped with a sieve drilled with 1 mm trapezoid holes and a 24-tooth rotor of 99 mm diameter.

At a rotor speed of 3000 rpm and an ambient temperature of around 20 °C, 50 g lots of *C. medica* and *L. acidissima* weighing approximately 2 kg were ground. Because the local temperature increase in plant elements during grinding is known to be improved at high rotor speed and to modify bioactive chemicals, this rotor speed was chosen as a compromise between the two [9]. The foundation of the sieving process is forcing granular materials through a 180 μm mesh sieve. The Analysette 3 Spartan equipment (Fritsch, Idar-Oberstein, Germany) was used to sift ground plants using vertical vibration. Following that, the plant powders were packed in polyethylene plastic bags and stored at 10 °C until analysis.

2.1.2. Plant extracts

Two kilograms of fresh *C. medica* and *L. acidissima* fruits and leaves were air-dried for two weeks, powdered, and extracted separately on cold with 5 L methanol then with increased polarity petroleum ether (pet.ether), methylene chloride (CH2Cl2), ethyl acetate (EtAc), and n-butanol (n-BuOH) then water, fractionation was carried out by solvent-solvent extraction.

First, we macerate 50 g for each plant part to test activity then we extract the most active on a large scale (2000,1400 &380 g) of fruits, leaves, and leaves powder of *L. acidissima* and *C. medica* respectively. The collected extract was completely dried under vacuum using a rotatory evaporator at 40 °C to yield the methanol extract was 11.90,16.50 and 15.50 g of fruits, leaves, and leaves powder of *L. acidissima* and *C. medica* respectively. Each weight was extracted successively. The collected extract was completely dried under vacuum using a rotatory evaporator at 40 °C to yield 0.29,0.5,0.75,1.4 and 8.0 & 1.15,0.57,1.21,4.38 and 7.6 and 1.08,0.36,0.59,6.27 and 8.2 g/g powder) respectively.

2.1.3. Chemicals and reagents

All chemicals used in the present study were purchased from Merck of high analytical grades. All extracts were kept in vials with dark glass at −20 °C up until further analysis.

2.2. Material for biological activity

2.2.1. In-vitro antiviral bioassay against H5N1 virus

2.2.1.1. Cells and virus. Toward assess the antiviral action of the investigated extracts reasserted avian influenza A virus (H5N1) remote from Egypt in 2013 A/CHICKEN/M7217B/1/2013 (H5N1) was utilized in this study. It was performed at the Center of

scientific excellence for Influenza Viruses, National Research Centre, Cairo, Egypt. Madin-Darby canine kidney (MDCK) cells used for virus spread were friendly and obtained from St. Jude Children's Research Hospital. In Dulbecco's modified Eagle medium (DMEM) containing 10 % fetal bovine serum and 1 % antibiotic-antimycotic mixture (penicillin-streptomycin-amphotericin B) the MDCK cells were routinely passaged.

2.2.2. Cytotoxicity assay for determination cytotoxic concentration (CC50) by (MTT assay) (10)

In DMSO at a concentration of 10 % in dH_2O (distilled H_2O) stock solutions of the test extracts were prepared. The stock samples were diluted with (DMEM) to the wanted concentrations. The cytotoxic activity of the extracts was tested in the MDCK cell line by using the 3-(4,5-dimethylthiazol-2-yl)-2,5-diphenyltetrazolium bromide (MTT) method [10,11] with minor modification. At a dual wavelength UV spectrometer at 540 nm with 620 nm reference wavelength an absorbance of formazan was detected. To calculate the concentration which exhibited 50 % cytotoxicity (CC50) the plot of % cytotoxicity versus sample concentration was used. The percentage of cytotoxicity compared to the untreated cells was determined with the equation given below. % Cytotoxicity versus sample concentration was used to calculate the concentration which exhibited 50 % cytotoxicity (CC50).

$$\%\ \text{Cytotoxicity} = \text{Absorbance of cell without treatment} - \text{Absorbance of cell with treatment}) \times 100$$

[12]

2.2.3. Plaque reduction assay for determination of antiviral activity [13]

To give 10^4 PFU/well A/Chicken/M7217B/1/2013 (H5N1) virus was diluted and mixed with the safe concentration of the tested extracts and incubated for 1 h at 37 °C before being added to the cells. The assay was passed out according to the method of Hayden et al. [10], in a six-well plate where MDCK cells (10^5 cells/ml) were cultivated for 24 h at 37 °C. The percentage reduction in plaque formation in comparison to control wells was recorded as follows: Control wells were included where the untreated virus was incubated with MDCK cells and finally, plaques were counted.

$$\%\ \text{inhibition} = \frac{\text{viral count (untreated)} - \text{viral count (treated)}}{\text{Viral count (untreated)}} \times 100$$

[13]

First, we investigate crude methanol extracts for fruits and leaves of both plants, then the fractions of most active extracts then combination between fractions (1:1) **1**: Petroleum ether soluble fraction (Pet.ether), **2**: methylene chloride soluble fraction (CH_2CL_2), **3**. Ethyl acetate soluble fraction (EtAc), **4**: *n*-butanol fraction (*n*-BuOH), **5**: water soluble fraction (H_2O).

2.3. UPLC-ESI-MS/MS study

The most active crude methanol fractions *C. medica* leaves (CML), *L. acidissima* leaves (LAL) and fruits (LAF) were analyzed for their content by UPLC/MS/MS (AB Sciex Triple TOF 5600+) [14]. Inject 25 μl MP-WS as a blank sample. Mobile phase working solution (MP-WS): DI-Water: Methanol: Acetonitrile – 50: 25: 25. We add 1 ml of MP-WS to 50 mg weighted sample. Vortex for 2 min followed by ultra-sonication for 10 min. Centrifuge for 10 min at 10000 rpm. 20 μl stock (50/1000 μl) was diluted with 1000 μl reconstitution solvent. Lastly, the injected concentration was 1 μg/μl. Inject 25 μl on positive mode and negative mode.

2.3.1. LC-QTOF parameters

In the mobile phase, two solvents were used for each mode: solvent (A) was deionized water with 0.1 % formic acid, solvent (B) was 5 mM ammonium formate buffer (pH 8) with 1 % methanol, and solvent (C) was 100 % acetonitrile. A Wa-ters reversed phase Exion Xbridge C18 column (2.1 × 50 mm, 3.5 μm) was used for LC separation. Prior to this, a Phenomenex precolumn with in-line filter disks (0.5 μm × 3.0 mm) was used.

Gradient Elution was carried out at 40 °C with a flow rate of 0.3 ml/min. From 0 to 1 min, the gradient was isocratic (90 percent (A) or (B), 10 % (C), and from 1 to 25 min, it was linear (90 percent to 10 % (A) or (B), 10 %–90 % (C). Solvents (A) and (C) were employed for the negative ion mode, and solvents (B) and (C) were utilized for the positive ion mode. 1000 μl of reconstitution solvent was used to dilute 20 μl of stock (50/1000 μl). Elution was isocratic (90 % (A) or (B), 10 % (C)) from 25.01 to 28 min. Only the negative ion mode was utilized with solvent (A), and only the positive ion mode was utilized with solvent (B). At last, 1 μg/μl was the injected concentration.

Conditions for mass spectrometry: negative ion mode; the run took 28 min and had 2584 cycles that lasted 0.6502 s each. The mass range that was found was 50–1000 Da. The nebulizer gas (GS1: nitrogen), drying gas (GS2: nitrogen), and curtain gas CUS flow rates for the MS1 acquisition were 45, 45, and 25 psi, in that order. The MS2 acquisition was used in conjunction with an 80 V decluttering potential, a 35 V collision energy CE, and a 20 V collision energy spread CES. The ion spray voltage was −4500 V and the temperature was 500 °C. Switch criteria were as follows; former target ions after 3 s and exclusion of isotopes within 2 Da. former ions were excluded after 3 repeats, Maximum numbers of candidate ions to monitor per cycle was 15. Positive ion mode; has same parameters but with ion spray voltage of 4500 V.MS-DIAL 3.52. Database used: Respect negative (1573 records) and positive (2737). Analysis parameters: Master View was utilized for feature (peaks) extraction from Total ion chromatogram (TIC) based on the following criteria: Features intensities of the sample-to-blank should be greater than 5. Features should have Signal-to-Noise greater than 5 (non-targeted analysis). Metabolites were assigned based on comparing the retention time (Rt.), MS data highly precise mass, molecular ion

Table 1
Identified metabolites in crude methanol extracts of *C.medica* leaves and *L.acidissima* fruits and leaves *via* UPLC/QTOF/MS-MS technique in negative. (−) and positive (+) ionization mode.

No.	Rt.	Molecular Formula.	Error (ppm)	Parent ion		Product ions (*m/z*)	Metabolites	CML		LAL		LAF		Class
				(M + H)	(M − H)			(−)	(+)	(−)	(+)	(−)	(+)	
1	1.09	C6H10O8	7.7	–	209	191(M-H-H_2O),129(M-H-2H_2O–CO2),85 (M-H-2H_2O–2CO_2)	Glucaric acid	+	–	–	–	–	–	Sugar acid
2	1.04	$C_6H_8O_7$	2.7	–	191	173(M-H-H_2O),129(M-H–H_2O–CO_2),111 (M-H-2H_2O–CO_2),87	Citric acid	+	–	+	–	+	–	Organic acid
3	1.06	$C_4H_6O_5$	2	–	133	115 (M-H-H_2O),71(M-H–H_2O–CO2)	Maleic acid	+	–	+	–	+	–	Organic acid
4	1.14	$C_6H_8O_7$	3.7	–	191	173 (M-H-H_2O),127 (M-H–H_2O–CO_2),111 (M-H-2H_2O–CO_2),85	Isocitric acid	+	–	+	–	+	–	Organic acid
5	1.3	$C_6H_{12}O_6$	8	–	179	161(M-H-H_2O),143 (M-H-2H_2O),125(M-H-3H_2O),71(M-H-2H_2O–CO_2–CO)	Glucose	+	–	+	–	+	–	Sugar
6	1.33	$C_{12}H_{22}O_{11}$	0.7	–	387 (M + HCOO /341	179(M-H-Glu.),161(M-H-Glu. -H2O),143 (M-H-Glu. -2H_2O),131 (M-H-Glu. –H2O–CH_2O)	Sucrose	+	–	+	–	+	–	Sugar
7	1.19	$C_{17}H_{20}O_9$	6.3	–	367	193,173	Feruloyl quinic acid	–	–	–	–	+	–	Phenolic acid
8	1.20	$C_7H_{10}O_5$	2.3	–	173	155 (M-H-H_2O),(M-H-CO_2)129,111(M-H–H_2O–CO_2),93(M-H–CO_2–2H2O)	Shikimic acid	+	–	–	–	+	–	Phenolic acid
9	1.23	$C_7H_{12}O_6$	1.3	–	191	147, 93,85	Quinic acid	+	–	+	–	+	–	Phenolic acid
10	1.31	$C_9H_8O_4$	9.2	–	179	161(M-H-H_2O),135(M-H–H_2O–CO)	Caffeic acid	+	–	+	–	+	–	Phenolic acid
11	1.34	$C_7H_6O_4$	2.6	–	153	109(M-H-COO)	Protocatechuic acid	–	–	+	–	+	–	Phenolic acid
12	1.49	$C_{18}H_{16}O_8$	1.2	–	359	197,179	Rosmarinic acid	+	–	+	–	–	–	Phenolic acid
13	2.06	$C_{10}H_{10}O_4$	8.8	–	193	149(M-H-CO_2),178(M-H-CH_3),134 (M-H–CO_2–CH_3)	Ferulic acid	+	–	–	–	–	–	Phenolic acid
14	2.60	$C_{16}H_{18}O_8$	3.5	–	337	191(Quinic acid),173(M-H-coumaroyl),163(coumaric acid),111	P-Coumaroyl quinic acid	+	–	–	–	–		Phenolic acid
15	1.96	$C_9H_8O_3$	–	165	163	119(M-H-CO2)	P-Coumaric acid	–	–	+	–	+	–	Phenolic acid
16	2.20	$C_{10}H_{10}O_4$	5.7	–	193	178(M-H-CH_3),149(M-HCOO),134(M-H–CH_3–CO_2)	Ferulic acid (3-(4-Hydroxy-3-methoxyphenyl) Prop-2-enoic acid)	–	–	+	–	+	–	Phenolic acid
17	2.61	$C_{16}H_{22}O_9$	2.5	–	357	195(M-H-glu.),151(M-H-glu-CO_2),136	Dihydro-feruloyl-*O*-glucoside	+	–	+	–	–	–	Phenolic acid
18	3.13	$C_7H_6O_5$	9	–	169	125	Gallic acid	–	–	+	–	+	–	Phenolic acid
19	3.40	$C_7H_6O_3$	9.5	–	137	93,65	*P*-Hydroxybenzoic acid	+	–	+	–	+	–	a phenolic derivative
20	3.71	$C_{10}H_{12}O_4$	1.7	–	195	177(M-H-H_2O),162(M-H–CO_2–CH_3),136 (M-H–H_2O–CH_3)	Dihydroferulic acid	–	–	+	–	–	–	Phenolic acid
21	4.50	$C_{16}H_{18}O_9$	5.6	355	–	163,145,135	Chlorogenic acid	+	–	–	+	–	+	Phenolic acid
22	4.52	$C_9H_8O_2$	6.4	–	147	129(M-H-H_2O),103(M-H-CO_2)	Cinnamic acid	+	–	+	–	–	–	Phenolic acid
23	6.91	$C_8H_8O_4$	0.5	–	167	152(M-H-CH_3)123(M-H-CO_2),108(M-H–CH_3–CO_2)	Vanillic acid	+	–	+	–	+	–	dihydroxybenzoic acid derivative
24	8.65	$C_{11}H_{12}O_5$	0.9	–	223	208(M-H-CH_3),193(M-H-2CH_3)	Sinapic acid (3-(4-Hydroxy-3,5-dimethoxyphenyl)-2-Propionic acid)	–	–	–	–	+	–	Phenolic acid
25	8.84	$C_8H_8O_3$	1.5	–	151	136,92	Vanillin	+	–	+	–	+	–	Phenolic aldehyde
26	11.02	$C_{11}H_{12}O_4$	2.1	–	207	192(M-H-CH_3),177(M-H-2CH_3),133	Sinapaldahyde	+	–	+	–	+	–	Phenols (Benzenoids)
27	13.12	$C_9H_{10}O_5$	1.9	–	197	182(M-H-CH_3),179(M-H-H_2O),153(M-H-CO_2),129,113,85	Syringic acid	+	–	+	–	–	–	Phenolic acid
28	2.29	C15$H_{10}O_5$	8.4	–	269	225,251	Apigenin	+	–	–	–	–	–	Flavonoid
29	5.45	$C_{27}H_{30}O_{15}$	4.5	–	593	473,309,285	Kaempferol 7- neohesperidoside	–	–	+	–	–	–	Flavonoid
30	5.52	$C_{27}H_{30}O_{15}$	2.5	–	593	473(M-H-120),327(M-H-120-146),298	Luteolin-8-C-β-D-glucopyranoside-7-*O*-rhamnoside	+	–	+	–	–	–	Flavonoid

(*continued on next page*)

Table 1 (*continued*)

No.	Rt.	Molecular Formula.	Error (ppm)	Parent ion		Product ions (*m/z*)	Metabolites	CML		LAL		LAF		Class
				(M + H)	(M − H)			(−)	(+)	(−)	(+)	(−)	(+)	
31	5.54	$C_{21}H_{20}O_{11}$	1	–	447	357(M-H-90),327 (M-H-120),339 (M-H-90-18),297(M-H-150)	Isoorientin (Luteolin -6-C-β-D-glucopyranoside)	+	–	+	–	+	–	Flavonoid
32	5.60	$C_{21}H_{20}O_{11}$	1.5	–	447	357(M-H-90), 327(M-H-120),297	Orientin (Luteolin-8-C-β-D-glucopyranoside)	+	+	+	–	–	–	Flavonoid
33	5.67	$C_{22}H_{22}O_{11}$	3.8	–	461	371 (M-H-90),341(M-H-120)	orientin -4′-methyl ether (Diosmetin-8-C-glucoside)	+	–	+	–	+	–	Flavonoid
34	6.06	$C_{15}H_{10}O_7$	6.7	–	301	283(M-H-H2O)	Quercetin	–	–	+	–	–	–	Flavonoid
35	6.10	$C_{27}H_{30}O_{14}$	1	–	577	457(M-H-120),311(M-H-120-146),293	Vitexin-2″-*O*-rhamnoside	+	+	+	–	–	–	Flavonoid
36	6.14	$C_{21}H_{20}O_{10}$	0.6	433	431	341(M-H-90),311(M-H-120),283	Vitexin (Apigenin 8-C-glucoside)	+	+	+	+	–	–	Flavonoid
37	6.26	$C_{27}H_{30}O_{14}$	0.4	579	577	341(M-H-90-146),323(M-H-90-146-18),293	Isovitexin 2″-*O*- rhamnoside	+	+	+	+	–	–	Flavonoid
38	6.40	$C_{21}H_{20}O_{10}$	4.3	–	431	413(M-H-H_2O),269 (M-H-Glu.)	Apigenin 7-glucoside	+	–	+	–	–	–	Flavonoid
39	6.58	$C_{21}H_{20}O_{10}$	0.2	433	431	413(M-H-H_2O),341(M-H-90),311 (M-H-120),283	Isovitexin (Apigenin 6-C-glucoside)	+	+	+	+	–	–	Flavonoid
40	6.64	$C_{21}H_{20}O_{12}$	2	–	463	301(M-H-glucose),271(M-H-Glucose-C02H)	Isoquercetin (quercetin-3-*O*-glucoside)	–	–	+	–	–	–	Flavonoid
41	7.77	$C_{28}H_{34}O_{15}$	1	611	609	303 (M + H-308),465,179,153	Hesperidin (hesperetin 7-*O*- rutinoside)	–	–	–	–	+	+	Flavonoid
42	7.79	$C_{27}H_{30}O_{16}$	3.2	–	609	301,300	Rutin	–	–	+	–	+	–	Flavonoid
43	8.95	$C_{15}H_{10}O_6$	8.8	287	–	245	Luteolin	–	+	–	–	–	–	Flavonoid
44	13.82	$C_{15}H_{14}O_6$	4	–	289	245(M-H-CO_2)	Epicatechin3,3′,4′,5,7 Pentahydroxyflavan)	+	–	–	–	–	–	Flavonoid
45	14.11	$C_{20}H_{20}O_7$	4.5	373	–	343 (M + H–2CH_3), 358 (M + H–CH_3)357 (M + H–CH_4),315 (M + H–2CH_3–CO)	Isosinensetin (5,7,8,3′,4′-Pentamethoxy flavone)	–	+	–	+	–	+	Flavonoid
46	9.30	$C_{15}H_{10}O_6$	1	–	285	267(M-H-H_2O),161,151,223,133	Kaempferol (3,4′,5,7-tetra hydroxyflavone)	–	–	+	–	–	–	Flavonoid
47	9.42	$C_{27}H_{30}O_{15}$	0.9	595	593	287(M + H-308)	Kaempferol-3-*O*-rutinoside	–	–	–	–	+	+	Flavonoid
48	10.31	$C_{15}H_{10}O_4$	6.3	–	253	235 (M-H-CH_3),209	Chrysin (5,7-Dihydroxy flavone)	–	–	+	–	–	–	Flavonoid
49	10.53	$C_{16}H_{12}O_6$	3	–	299	284(M-H-CH_3),137	Chrysoeriol(4′,5,7-trihydroxy-3′-methoxy flavone)	–	–	+	–	–	–	Flavonoid
50	10.67	$C_{15}H_{10}O_5$	5.4	–	269	251,225,197,149	Apigenin	+	–	+	–	–	–	Flavonoid
51	10.94	$C_{17}H_{14}O_8$	2	–	345	330(M-H-CH_3),315(M-H-2CH_3),276(M-H-3H_2O–CH_3)	Limocitrin(4′,5,7-trihydroxy-3′,8-dimethoxy flavonol)	–	–	–	–	+	–	Flavonoid
52	12.10	$C_{19}H_{18}O_6$	2.9	343	341	328(M + H–CH_3),313(M + H–CH_2O),299 (M + H–CH_4–CO),283(M + H–4CH_3),282 (M + H–2CH_2O–H)	4′,5,6,7-tetramethoxy flavone	–	–	+	+	–	+	Flavonoid
53	12.35	$C_{20}H_{20}O_8$	0.9	389	–	374(M + H–CH_3),359(M + H–CH_2O),341 (M + H–3CH_4),227(RDA, ring B)	6-Hydroxy3′,4′,5,7,8pentamethoxy flavone	–	–	–	–	–	+	Flavonoid
54	14.12	$C_{21}H_{22}O_8$	2.9	403	–	388(M + H–CH_3),373(M + H-(CH_2O),211 (RDA, ring A),183(211-CO),163 (RDA, ring B)	Nobiletin	–	+	–	+	+	+	Flavonoid
55	14.20	$C_{19}H_{18}O_6$	1.7	343	–	328 [M + H–CH_3], 313 [M + H–2CH_3],299(M + H–CO_2), 285 [M + H–2CH_3–CO.	Tetramethyl-*o*-isoscutellarein	–	–	–	+	–	+	Flavonoid
56	14.88	$C_{22}H_{24}O_9$	1.7	433	–	418 (M + H–CH_3),403(M + H–2CH_3),385 (M + H–2CH3–H2O),211	Heptamethoxy flavone	–	–	–	–	–	+	Flavonoid
57	15.21	$C_{20}H_{20}O_7$	1.5	373	–	358 [M + H–CH_3],343 [M + H–2CH_3], 329 [M + H–CO_2].	Sinesetin (3′,4′,5,6,7-pentamethoxy flavone)	–	+	–	+	–	+	Flavonoid

(*continued on next page*)

Table 1 (*continued*)

No.	Rt.	Molecular Formula.	Error (ppm)	Parent ion		Product ions (*m/z*)	Metabolites	CML		LAL		LAF		Class
				(M + H)	(M − H)			(−)	(+)	(−)	(+)	(−)	(+)	
58	15.24	$C_{20}H_{20}O_7$	2.9	373	–	358(M + H–CH_3),343(M + H–CH_2O),211 (RDA,ring A),183(211-CO)	Tangeretin (4′,5,6,7,8-Pentamethoxyflavone)	–	–	–	+	–	+	Flavonoid
59	15.27	$C_{20}H_{20}O_7$	1.1	373	–	358(M + H–CH_3),343(M + H–2CH_3),315 (M + H–2CH_3–CO)	Isosinensetin (5,7,8,3′,4′-Pentamethoxyflavone)	–	+	–	+	–	+	Flavonoid
60	19.46	$C_{18}H_{16}O_5$	3.2	313	–	298 (M + H–CH_3), 297 (M + H–CH_4), 270 (M + H–CH3–CO), 269 (M + H–CH_4–CO), 255 (M + H–2CH_3–CO)	5,7,4′-Trimethoxyflavone	–	+	–	+	–	–	Flavonoid
61	1.18	$C_{11}H_{10}O_4$	3.2	–	205	187,173,143,131,111,87	Limettin (5,7-dimethoxy coumarin) (Citropten)	–	+	–	–	+	–	Coumarins
62	2.36	$C_9H_6O_4$	1	179	177	161(M + H–H2O),151(M + H–CO),121 (M + H–CO–CH2O)	Esculetin (6,7-Dihydroxycoumarin)	–	+	–	–	+	+	Coumarins
63	4.47	$C_{15}H_{16}O_9$	0.8	–	339	321(M-H-H_2O),293 (M-H-H_2O),177(M-H-Glu),131 (M-H-Glu.–CO–H_2O)	Esculin (6,7-dihydroxy coumarin 6-glucoside)	–	–	–	–	+	–	Coumarins
64	7.04	$C_{10}H_8O_4$	3.5	193	191	176(M-H-CH_3),148(M-H–CH_3–CO)	Scopoletin	+	+	+	+	+	+	Coumarins
65	7.96	$C_9H_6O_4$	1	179	–	161(M + H–H_2O),133(M + H–CO–H_2O)),119 (M + H–CH_2CO–H_2O)	Daphnetin (7,8 dihydroxycoumarin)	–	+	–	+	–	+	Coumarins
66	9.65	$C_{14}H_{14}O_4$	3.8	247	–	229(M + H–H_2O),175,147	Columbianetin	–	–	–	+	–	+	Coumarins
67	10.0	$C_{14}H_{14}O_4$	9.9	247	245	227(M-H-H_2O),175	Marmesin	–	–	+	+	+	+	Coumarins
68	10.11	$C_9H_6O_2$	3.2	147	–	103,91,77	Coumarin	–	+	–	+	–	+	Coumarins
69	10.73	$C_{10}H_8O_3$	9.2	177	–	162(M + H–CH_3),149(M + H–CO),134(M + H–CO–CH_3)	7-hyroxy 4-methyl coumarin (hymecromone)	–	+	–	+	–	+	Coumarins
70	11.27	$C_{15}H_{16}O_3$	2.6	245	–	230(M + H–CH_3), 215(M + H–CH_2O),212 (M + H–CH_2O–H2),203 (M + H–C_3H_6),187(M + H–CO–CH_2O)	Osthol	–	+	–	+	–	–	Coumarins
71	11.46	$C_{11}H_6O_3$	8.3	187	–	143,131,115	Psoralen	–	+	–	+	–	+	Coumarins
72	11.91	$C_{12}H_8O_4$	8.1	217	–	202,185,174	Xanthotoxin	–	+	–	+	–	+	Coumarins
73	12.46	$C_{11}H_{10}O_4$	1	207	–	192 (M + H–CH_3),164(M + H–CH_3–CO),149(M + H–CO–CH_2O),121 (149-CO)	6,7-dimethoxy coumarin	–	+	–	+	–	+	Coumarins
74	13.06	$C_{12}H_8O_4$	1	217	–	202 (M + H–CH_3),174 (M + H–CH_3–CO)	Bergapten	–	+	–	+	–	+	Coumarins
75	14.70	$C_{14}H_{14}O_3$	0.9	231	–	175,147	Osthenol	–	–	–	+	–	+	Coumarins
76	15.16	$C_{14}H_{12}O_3$	7.2	229	–	213,211,185	Seselin	–	–	–	+	–	–	Coumarins
77	8.14	$C_{26}H_{30}O_{10}$	3.2	–	501	457(M-H-CO_2),413(M-H-2CO_2),433,372,327	Limonexic acid isomer	–	–	–	–	+	–	Limonoids
78	8.42	$C_{26}H_{30}O_{10}$	3	–	501	457(M-H-CO_2),439(M-H–CO_2–H_2O),433,413(M-H-2CO_2)	Limonexic acid (Limonexin)	–	–	–	–	+	–	Limonoids
79	19.79	$C_{26}H_{28}O_9$	5.6	485	–	217(M + H-ring C, D, Furan-H_2O),203 (217-CO_2),189(M + H-ring A, B, C)	Limonin diosphenol	–	+	–	+	–	–	Limonoids
80	7.57	$C_{18}H_{32}O_5$	3.5	–	327	309(M-H-H_2O),229((M-H-3H_2O–CO_2),211,171	Trihydroxy octadecadienoic acid	+	–	+	–	–	–	Fatty acid

Rt: Retention time M.F.: Molecular formula +: present, -: absent CML: *C. medica* leaves LAL: *L. acidissima* leaves LAF: *L. acidissima* fruits.

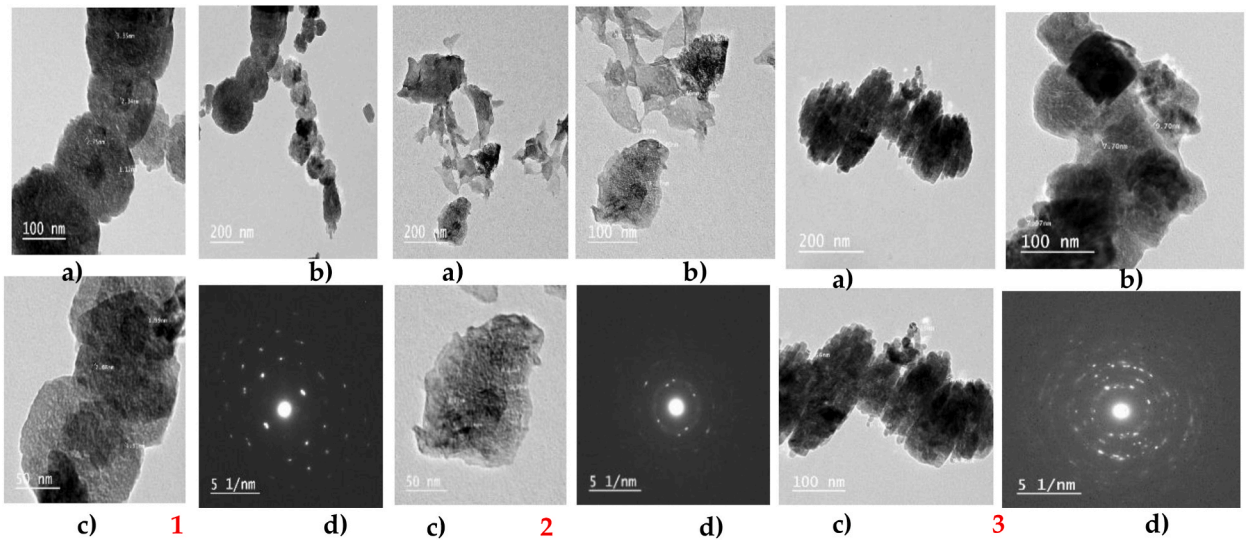

Fig. 1. TEM analysis of ZnONPs nanoformulation for 1) LAL, 2) LAF and 3) CML.

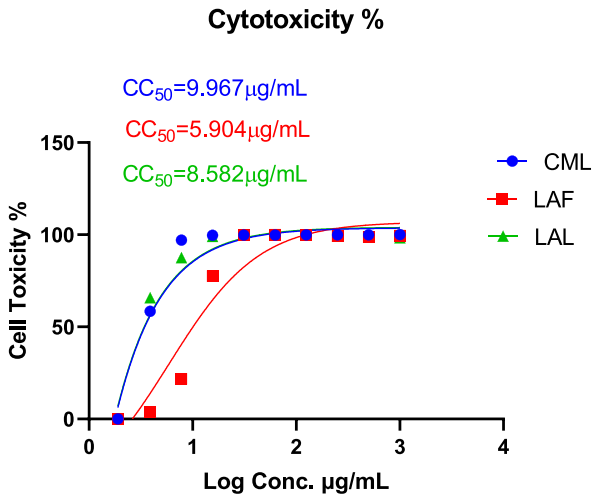

Figure (2). In MDCK cells cytotoxicity assay of the tested extracts. Cytotoxic Concentration (CC50) for ZnONPs nano formulation of *C. medica* leaves and *L. acidissima* fruits and leaves based on the dose–response was determined using MTT. Using nonlinear regression analysis of GraphPad Prism software (version 5.01) the 50 % cytotoxic concentration (CC50) was calculated for each compound.

Table 2
Antiviral activity measured using Plaque reduction assay for ZnONPs of *C. medica* leaves and *L. acidissima* fruits and leaves.

Extract	Conc. µg/ml	Virus Control (PFU/ml)	Viral Count Post- Treatment (PFU/ml)	Viral Inhibition %
CML	10	$6.5 * 10^6$	$5.0 * 10^6$	23.1 %
	5		$5.3 * 10^6$	18.5 %
	2.5		$5.7 * 10^6$	12.3 %
	1.25		$6.0 * 10^6$	7.7 %
LAF	10	$6.5 * 10^6$	$3.5 * 10^6$	46.2 %
	5		$4.0 * 10^6$	38.5 %
	2.5		$4.0 * 10^6$	38.5 %
	1.25		$5.0 * 10^6$	23.1 %
LAL	10	$6.5 * 10^6$	$4.5 * 10^6$	30.8 %
	5		$5.0 * 10^6$	23.1 %
	2.5		$5.5 * 10^6$	15.4 %
	1.25		$6.0 * 10^6$	7.7 %

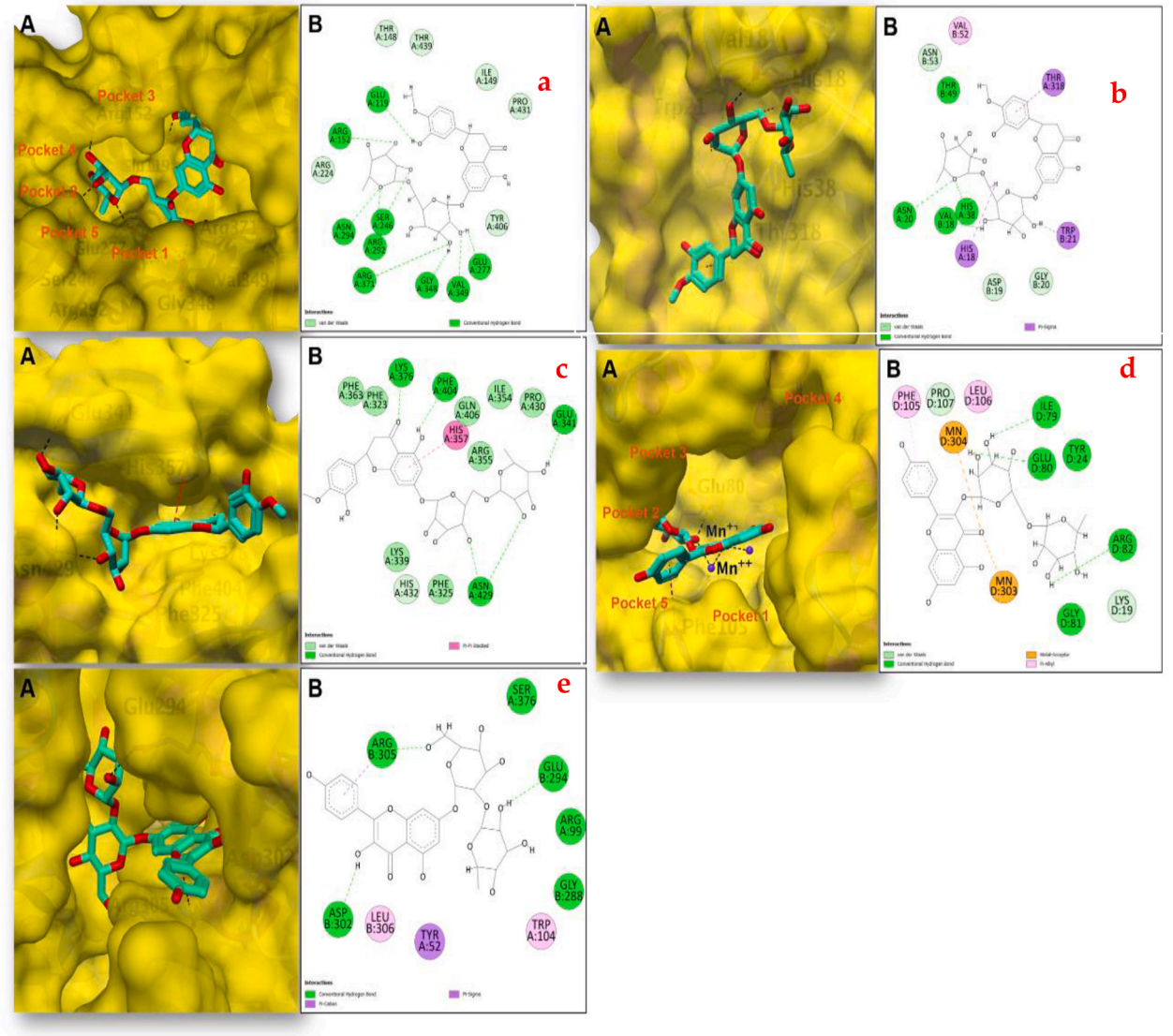

Fig. 3. [**a**]: (A): The 3D illustration of the best docking pose of hesperidin into the active site of NA (PDB ID: 3TI6). (B): 2D illustration of the binding interactions of hesperidin with the key amino acid residue. [**b**]: (A): The 3D illustration of the best docking pose of hesperidin into the active site of HA (PDB ID: 6CF7). (B): 2D illustration of the binding interactions of hesperidin with the key amino acid residue. [**c**]: (A): The 3D illustration of the best docking pose of hesperidin into the active site of PB2 (PDB ID: 4CB4). (B): 2D illustration of the binding interactions of hesperidin with the key amino acid residue. [**d**]: (A): The 3D illustration of the best docking pose of Kaempferol-3-*O*-rutinoside into the active site of PA (PDB ID: 4E5H). (B): 2D illustration of the binding interactions of (Kaempferol-3-*O*-rutinoside with the key amino acid residue [**e**] (A): The 3D illustration of the best docking pose of Kaempferol 7- neohesperidoside into the active site of NP (PDB ID: 3RO5). (B): 2D illustration of the binding interactions of Kaempferol 7- neohesperidoside with the key amino acid residue.

fragmentation model, the predicted formulas data in the literature and databases listed in the authorized websites; Mass bank of North America (MoNA) and PubChem together with the data base (Peak view software program) provided from the metabolomics unit, Basic Research Department, Egypt, Cairo, Children's Cancer Hospital (57357). The ionization of compounds in our study was achieved in the negative and positive ionization modes.

2.4. Preparation of nanoparticles

2.4.1. Green preparation of metal (zinc oxide) nanoparticles

ZnONPs were manufactured from the *L. acidissima* leaves (LAL) and fruits (LAF) and *C. medica* leaves (CML) methanol extract by a process illuminated previously by Attia et al. [15], After centrifuging the produced ZnONPs at 4000 rpm, they were cleaned twice in ethanol and twice in bi-distilled water to produce pellets of nanoparticles that could be freeze-dried.

2.4.2. Structural and morphological characterization of metal nanoparticles [16]

Additionally, the powdered sample was exposed to radiation from a CuKα1-X Ray diffractometer (λ = 15406) running at 40 kV and 30 mA with 2θ varying from 20 to 90° in order to confirm the presence of ZnO crystals and define their size and structure. The ZnONPs were principally investigated using UV-1601 (Shimadzu Corporation, Japan) by UV–visible spectroscopy ranging between 200 and 600 nm. Then, attenuated total reflectance mode was used to conduct FTIR analysis using a Jasco FTIR 4100 spectrophotometer (Japan). The functional groups and different phytochemical substances in charge of the creation and stabilization of the nanoparticles were categorized using FTIR.

2.4.3. Particle size and zeta potential

Size distribution, average diameter, and zeta potential of samples were measured by using a particle size analyzer (Nano-ZS, Malvern Instruments Ltd., UK). For determining zeta potential, just before assessment the sample was sonicated for 30–60 min.

2.4.4. Electron microscope

Determination of morphology and particle size of ZnONPs mediated by *L. acidissima* leaves and fruits and *C. medica* leaves extract was performed usingTransmission Electron Microscope (TEM) (JEOL-JEM-1011, Japan).

2.5. Molecular docking study

To framework the chemical structures of the separated compounds then energy minimized by MMFF94x Force Field in gas phase to a gradient of 0.01 kcal/mol.Å also saved in PDBQT format the ChemBioDraw Ultra 14.0 software (Cambridge Soft corporation) was used. Five co-crystal structures (PDB ID: 3TI6, 6CF7, 4E5H, 4CB4 and 3RO5) represent the five key influenza virus targets, were recovered from the protein data bank, and involved in our molecular docking simulation. Molecular Graphics Laboratory (MGL) tools v1.5.7 used for all target proteins preparation to achieve deletion of water molecules and other atoms, addition of polar hydrogens, and addition of Kollman Charges then saved in PDBQT format. Grid boxes were adjusted at the co-crystalized ligands and their dimensions were set to accommodate the whole active sites of the target proteins. The docking poses were rated according to their docking scores, and the best energy pose was selected. All Docking calculations were implemented by the aid of the open-source software Auto Dock vina v1.1.2. Using Discovery Studio Visualizer v21.1.0.20298 the interactions among the screened compounds along with the target proteins were analyzed [17].

2.6. Statistical analysis

The 50 % cytotoxic concentration (CC50) was calculated for each compound using nonlinear regression analysis of GraphPad Prism software (version 5.01). All analytical values shown represent the means of three replicates.

3. Result and discussion

3.1. In vitro antiviral activity against (H5N1)

Results of antiviral activity against (H5N1) (Plaque reduction assay) presented in table (S1) showed the potency in descending order is LAL > LAF > CML methanol extracts at concentration 160 μg (the optimum tested dose for activity). The antiviral activity of the fractions of most potent extracts table (S2) showed decrease in the activity due to loss of synergism effect of phytochemicals so combinations between fractions was done to increase activity and to show the fraction that may be responsible of higher activity. Consequently, table (S3) revealed a rise in antiviral activity in combination comprising CH_2Cl_2 in LAL extract, pet. ether in LAF followed by CML extract. Currently, there is no treatment for viral diseases. Results obtained here agree with the previously reported data [15–17]. *In vitro* antiviral screening of 25 extracts of medicinal plants using different solvents and isolated compound methyl gallate was previously carried out. The antiviral activity was measured by focus-forming unit assay, quantitative real-time RT-PCR, and immunofluorescence assays [18]. Our study is considered as ongoing searching for natural antiviral agents. The antiviral activity against avian influenza A (H5N1) and COVID-19 virus of *Citrus* species was previously tested [3,19]. Crude extracts of some Asian medicinal plants obtained by both water and ethanol extractions were *in vitro* investigated antiviral activity on H5N1 virus infection. *Curcuma longa* and *aempferia parviflora* exhibited robust anti-H5N1 activity [20].

3.2. In-vitro cytotoxicity assay (TC50)

In-vitro cytotoxic assay for the methanol soluble extracts of the fruits and leaves of *C. medica* and *L. acidissima* in table (S4) revealed that CML had low cytotoxicity while CMF &LAF methanol extracts had high cytotoxicity. The fruits of both *C. medica* and *L. acidissima* exerted high cytotoxicity which may be attributed to their antioxidant constituents as flavonoids [18]. So, study of chemical composition of these most potent extracts was carried out to correlate with this activity. Then, fractionation was done for the three active methanol extracts (CML, LAL&LAF) with solvent with increasing polarity then cytotoxic activity and antiviral (Table S5) activities were repeated. Beforehand *C. longa, K. parviflora, and Psidium guajava* were examined also for their cytotoxicity in the Madin-Darby canine kidney cells. Whereas *C. longa* and *K. parviflora* showed strong anti-H5N1 activity [21].

3.3. UPLC-ESI-–Q-TOF–MS-MS. Characterization of active methanol extracts of C. medica leaves, L. acidissima fruits and leaves

The CML, LAL, and LAF crude methanol extracts were exposed to UPLC-ESI-Q-TOF-MS-MS, which considered the most widely rapid, sensitive available and commonly used technique for the identification of different metabolites. The identified compounds and their mass fragments as well as molecular formula are listed in Table (1), where they numbered according to their retention times in the obtained chromatograms as shown Figs. S1–3. Illustration of different chromatographic peaks allowed the identification of compounds according to the retention time and the exact mass-to-charge ratio (*m/z*) and by comparing to the previous published data.

A total of 48,74&74 chromatographic peaks (Table 1 & Figs. S1–3) belonging to various metabolite classes were derived in methanol extract of CML LAL&LAF, respectively including phenolic acids flavonoids and their derivatives which represented the major compounds ionized mainly in the negative ion mode gave fragments from $[M-H]^-$ ion followed by, coumarins in the positive ion mode $(M+H)^+$ as well as methylated flavonoids, sugars compounds. Identified compounds from methanol extract of CML are like that identified in methanol extracts of LAL and LAF except in five compounds which are Glucaric acid, *P*-Coumaroyl quinic acid, Diosmetin 8-C-Glucoside-6-C-pentoside, Epicatechin and luteolin as shown in Table (1). Important groups of flavonoids were reported. Flavonoids derived from the citrus family want to be measured from a therapeutic, nutraceutical, and pharmaceutical opinion of view for upcoming medication [21,22]. High-resolution mass spectrometry, permitting the recognition of 24 compounds phenolic in nature and 5 limonoids in numerous peels of citrus species. Several compounds comprising quinic, malic, citric, protocatechuic acid, sucrose, esculetol and catechol were detected [23]. 4-hydroxybenzaldehyde, luteolin-6, 8-di-C-glucosidchrysoeriol-6,8-di-C-glucoside, eriocidin, *p*-hydroxycinnamic acid, diosmetin-6-C-glucoside, coumarins; scopoletin and its isomers, azelaic acid, isofraxidin and its isomers, nomilinic acid, deacetylnomilinic acid, heraclenin, (E, E)-9-oxooctadeca-10, 12-dienoic acid and ricinoleic acid were first discovered from *C.medica* [23] which provide findings that are equivalent to those of our research.

3.3.1. Flavonoids

Flavonoids represented the major metabolites identified in both plant parts under investigation and their fragmentation patterns could be annotated. Briefly, the characteristic fragmentation ions of *O*-glycosides were exposed over the loss of (162 amu) signified hexose (glucose or galactose) or loss of (146 amu) for deoxy sugar (rhamnose) or loss of (132 amu) for pentose (arabinose or xylose) while fragmentation ions of C-glycosides characterized by (0,2) or (0,3)-ring cleavages and dehydration [24].

Peak 54 in Table 1 which represent 5,6,7,8,3′,4′-Hexamethoxy flavone(nobiletin) whose molecular weight in positive mode is (403) + peak 388 appear due to loss of methyl group ($M+H-CH_3$), peak 373 due to loss of CH_2O group ($M+H-CH_2O$), peak 211(RDA,ring A), peak 183(211-CO)and peak163 (RDA, ring B) [25].

Peak 39 in Table 1 represent Isovitexin (Apigenin-6-C-glucoside) an example of C- glucoside whose molecular weight appear at $(431)^-$ in negative mode and (433)+ in positive mode fragmentation illustrated in negative mode as peak 413 appear due to loss of H_2O molecule ($M-H-H_2O$), peak 341 appear due to ring cleavage (M-H-90), peak 311 appear due to ring cleavage (M-H-120) [26]. 4-hydroxybenzaldehyde, luteolin-6,8-di-C-glucosid, eriocidin, chrysoeriol-6, diosmetin-6-C-glucoside and 8-di-C-glucoside were previously reported [23].

3.3.2. Coumarins

Appears mainly in positive ion mode as peak 64 (Table 1) represent scopoletin whose molecular weight $(191)^-$ in negative mode and (193)+in positive mode peak 178 appear owing to loss of methyl group ($M+H-CH_3$), peak 150 appear due to loss of CO group ($M+H-CO$), while peak 133 appear owing to loss of CH_3COOH group ($M+H-CH_3COOH$) [27]. *p*-hydroxycinnamic acid, scopoletin and its isomers [23].

3.4. Characterization of prepared nano emulsions

3.4.1. Preparation of nanoemulsions

The nanoemulsions (ZnONPs) were prepared using the method of Rupa et al. [28]. After the formation of the nanoemulsions, the LAF, CML, and LAL crude methanol extracts each (200 μg/mL) were dissolved in the prepared nanoemulsions by stirring then nanoparticles were categorized using transmission electron microscopy (TEM), zeta potential measurement, and polydispersity index (PDI).

3.4.2. Calculation of particle size and polydispersity index (PDI)

By the method mentioned by Niknam et al., [29], size and size distribution of the prepared nanoemulsions of LAL, LAF and CML extracts were determined. The z-average diameter documented for the prepared nanoemulsions were 919.9 ± 276.8 with PDI of 0.196 for LAL, 883.2 ± 68.42 with PDI of 0.593 for LAF and 2511 ± 70.92 nm with PDI of 0.729 for CML. High microemulsion stability for LAL evidenced by the small particle size with its narrow distribution and explains the isotropicity and clarity of the formulation.

3.4.3. Characterization of optimized nanoemulsions by (TEM)

Using TEM (transmission electron microscopy) the morphology of the prepared nanoemulsions of LAL, LAF and CML extracts were characterized at an acceleration voltage of 80 KeV. The TEM micrograph of the ready nanomulsions is shown in Fig. 1, dark droplets were detected, virtually spherical in shape with the option to notice the outermost layer. Observation of dim droplets was mainly owing to the strong interaction between the sample and the phosphotungstic acid used in staining the droplets which approves the observation of Sahiro et al., [30]. We observed the formation of flocs in the nano-emulsions. which maintains the integrity of the

droplets, which is fundamentally different from the process of coalescence [31].

3.4.4. Characterization of prepared nanoemulsions by zeta potential measurement

Surface charge of the prepared nanoemulsions were determined by zeta potential dimensions recorded −5.11, 17.3 and −7.44 mV for LAL, LAF and CML extracts respectively by using MeOH as dispersant (Fig. S4). Zetapotential is considered a useful parameter to measure surface charge of droplets and predict the dispersion stability of prepared nanoemulsion as negative value confirms the repulsion among the particles and prove the good stability of the prepared nanoemulsion [32]. Our results clearly indicated that the particles are negatively charged and stable due to the electrostatic repulsion as the value of zeta potential should be greater than 30 mV or less than −30 zeta potential is required for an indication of stable nanosuspension [23].

3.4.5. UV spectroscopy

Aqueous extracts of leaves and fruits of *L. acidissima* and leaves of *C. medica* were subjected to UV measurements between 200 and 600 nm. ZnONPs synthesized from LAL, LAF, and CML extracts were shown to have a high absorption peak at 368 nm (Fig. S5), indicating the formation of ZnONPs. ZnO has shorter wavelengths at the nanoscale than ZnO seen in conventional ZnO, which is consistent with studies supporting material oxides' shorter wavelengths. The transition of the electronic cloud on the overall skeleton of the ZnONPs may be responsible for the broadness of absorption. The ZnONPs' absorption in the UV spectrum indicates that the nanoparticles may find use in a variety of medicinal applications, including sunscreen protectors and antibacterial ointments.

3.4.6. Fourier transform infrared spectroscopy (FTIR)

At 400–4000 cm^{-1} the FTIR was analyzed to identify the several functional groups current in the nanoparticles and LAL, LAF and CML extracts. Regarding ZnONPs, a strong absorption peak at 3748 cm^{-1} indicated OH group accountable for the water adsorption on the ZnONP surface. Band existing at 895 or 913 cm^{-1} was designated to the bending vibration of alkane groups. The occurrence of CO group of ethers, carboxylic acid esters and alcohols signified by absorption peaked at 1050 cm^{-1}. FTIR spectrum for LAL, LAF and CML extracts (Fig. S6) displayed a significant peak at 3385 cm^{-1}, indicating the existence of phenolic or alcoholic OH groups. The representative peaks of the ZnONPs were given at 457 and 442 cm^{-1}. Medium bands observed at 2924 and 2853 cm^{-1} revealed the incidence of alkane groups. The evident peaks at 1615, 1514 and 1455 cm^{-1} in the alcoholic extract (Fig. S7) specified the presence of cyclic C–C or C═O stretch of polyphenolic compounds shifted to 1582 cm^{-1} in ZnONPs because of the bond between the polyphenols and NPs. The alkenes (=C–H) group was represented by the moderate bond that appeared at 835 cm^{-1} and the weak peaks at 673 cm^{-1}. The intense peak acquired at 1067 or 1009 cm^{-1} proved the presence of alkane groups.

3.4.7. X-ray diffraction (XRD)

The framework for the examination of ZnONP structural features was established by X-ray diffraction (XRD). at position 20° the XRD diffraction peaks were seen at 2θ v spectra of LAL ZnONPs (Fig. S8a) the peaks are 31.77, 34.42, 36.25, 47.51, 56.56, 62.81, 66.36, 67.91, 69.02, 72.5, 76.85 and 81.30. while spectra of LAF ZnONPs (Fig. S8b) the peaks are 31.56, 31.74,34.42, 36.27, 47.36, 56.40, 59.08, 62.71, 67.74, 68.99 and 76.62 and CML ZnONPs (Fig. S8c) 31.69, 34.38, 36.20, 47.58, 56.48, 62.87, 66.34, 67.83, 69.02, 72.53, 76.81 and 81.28. these results show highly pure hexagonal structure of ZnONPs [33]. Moreover, ZnONPs were believed as impurity-free since their peaks on the XRD were the only atypical ones.

[34]. Comparable to (100), (002), (101), (102), (110), (103), (200), (112), (201), (004). (202), (104), and (203), respectively. Based on green chemistry views, the green synthesis of metal nanoparticles should include three primary steps: 1) choosing a biocompatible and nontoxic solvent medium, 2) taking environmentally friendly reducing agents, and 3) taking nontoxic chemicals for nanoparticle stabilization. As of its numerous applications and distinctive features, scientists have recently discovered the significance of zinc oxide (ZnO). ZnONPs, unlike other nanoparticles, have better biocompatibility with human cells than zinc metal and are easily absorbed by biological tissues. Nanoparticles containing ZnO have attracted a lot of attention and are now used in a variety of industries, including packaging and food additives. ZnONPs also have antiviral action against a wide variety of viruses, including SARS-CoV-2 and many types of respiratory viruses and herpes viruses [35].

3.5. Antiviral activity for ZnONPs

3.5.1. In- vitro cytotoxic activity for ZnONPs

In comparison with the cytotoxic activity in table (S4,5) we found that the cytotoxicity of ZnONPs for leaves extract of *C. medica* and *L. acidissima* leaves and fruits extracts is significantly higher than that of the methanolic extracts as presented in Figure (2).

3.5.2. In vitro antiviral activity (plaque reduction assay) for ZnONPs

After cytotoxicity assay in table (S5), these concentrations were chosen to be used for plaque reduction assay dose-dependant antiviral activity of ZnONPs of leaves *C. medica* and *L. acidissima* fruits and leaves as shown in Table (2), where the activity of ZnONPs of *L. acidissima* fruits is higher than that of ZnONPs of both *L. acidissima leaves* and *C. medica* leaves at the same concentration which may be attributed to its phenolic metabolites. As well nano formulation of *L. acidissima* fruits enhance the observed antiviral activity [14,16].

The activity of ZnONPs of *L. acidissima* fruits is more than that of ZnONPs of both *L. acidissima* leaves and *C. medica* leaves at the same concentration. ZnONPs also have antiviral action against a variety of viruses, including SARS-CoV-2 and many types of respiratory viruses and herpes viruses [35,36].

3.6. Molecular docking

For authentication of the employed docking protocol, the co-crystalized ligands associated with our target proteins NA (PDB code: 3TI6), HA (PDB code: 6CF7), PA (PDB code: 4E5H), PB2 (PDB code: 4CB4) and NP (PDB code: 3RO5) have been re-docked to their binding sites and RMSD was calculated. The docking protocol has succeeded in reproducing the original binding pose for each ligand with RMSD values 0.43, 0.94, 0.30, 0.30 and 0.32 Å respectively.

Eighty compounds that have been identified by LC-MS from the biologically active extracts of both inspected plants have been subjected to docking simulation against five key proteins in survival and replication of influenza virus [37,38]. Among the docked compounds, the eight identified flavonoid di-glycosides have shown outstanding affinity toward the five examined proteins and achieved docking scores which move toward or even exceeded that achieved by reference compound (oseltamivir) and by the native ligands after re-docking in their original binding pockets (Table S6). Compound 41(Hesperidin) has demonstrated the best binding affinity toward NA, HA ang PB2 (−10.675, −8.131 and −10.046 kcal/mol respectively). Compound 41 interacted with the active site of NA through formation of seven hydrogen bonds by its sugar part with residues Arg292, Gly384 and Arg371 in pocket 1 and residues Ser246 and Glu277 in pocket 5 and Arg152 in pocket 3 and Val349. On the other hand, the aglycone part which extended inside pocket 2 formed a single hydrogen bond with Glu119 (Fig. 3a). Regarding its interaction with HA, compound 41 was stabilized in the active site by two hydrogen bonds and two CH-π stacking between the sugar part and the residues Val18, His38, His18 and Trp21 and additional CH-π stacking between the aglycone part B ring and Thr318 (Fig. 3b). Compound 41 has been oriented in the PB2 cap binding site in a way resembling that of the co-crystalized ligand where the aglycone A and C rings lied horizontally sandwiched between the aromatic residues His357, Phe323, Phe325 and Phe404 and formed two hydrogen bonds with Phe404 and Lys376 and π- π stacking with His 357 while the sugar part formed additional three hydrogen bonds with Glu341 and Asn429 (Fig. 3c). Moreover, compound 47(Kaempferol-3-*O*-rutinoside) has shown the highest binding affinity toward PA binding site (−10.097 kcal/mol). The aglycone A and C rings in addition to the proximal sugar moiety of compound 47 have occupied the center of binding site where the two crucial Mn^{2+} cations are present, and three metal interactions were formed by the ring C carbonyl group and one sugar hydroxyl group with the two Mn^{2+} cations. Furthermore, the proximal sugar moiety formed two other hydrogen bonds with Ile79 and Glu80 while the aglycone ring B which extended in pocket 5 and formed CH-π stacking with Phe105 and the distal sugar moiety which extended deeply in pocket 2 formed one hydrogen bond with Arg82 (Fig. 3d). Finally, compound 29 (Kaempferol 7- neohesperidoside) which has achieved the highest binding affinity against NP (−11.263 kcal/mol) was perfectly inserted in the binding pocket between the two NP monomers and interacted strongly with the binding site residues through formation of two hydrogen bonds by two sugar hydroxyl groups with Glu294 and Arg305 in addition to another hydrogen bond formed between the aglycone ring C hydroxyl group and Asp302 and CH-π stacking between aglycone ring B and Arg305 (Fig. 3e).

The above conclusions suggest that the biologically active extracts can apply its antiviral effect against influenza virus through inhibition of these five key proteins mainly by its content of flavonoid di-glycoside particularly compounds 29, 41 and 47(Table 1).

The study is extensive, including **Citrus medica** var. *sarcodactylis* Swingle and **Limonia acidissima** L., for both fruits and leaves extracts concentrating on their antiviral activity against the avian influenza H5N1 virus. It also incorporates the study of zinc oxide nanoparticles formulations (ZnONPs) together with the natural extracts. Utilizing UPLC-QTOF–MS-MS, a detailed comparative phytochemical analysis of **C. medica** and **L. acidissima** leaves and fruits was carried out. This advanced technology helped in identifying the complex phytochemical components effectively. The study doesn't stop at merely identifying the antiviral activity; it further validates these effects through molecular docking. This approach provided evidence of the substantial potential of using these extracts as medicinal agents against the virus, presenting a scientifically sound method by showing how these natural compounds interact with virus proteins. The study distinctly outlines the antiviral potency in an ascending order: **L. acidissima** leaves (LAL) > **L. acidissima** fruits (LAF) > **C. medica** leaves (CML), providing clear insights into which extracts have higher efficacy. Such a hierarchy is valuable for further research and application. Highlighting the nanoformulation of LAF as having the most remarkable antiviral effects introduces a novel approach to enhancing the effectiveness of natural extracts against viruses. The identification of diverse chromatographic peaks through metabolomic profiling for **C. medica** fruits (CMF) and **L. acidissima** leaves (LAL) underline the complexity and richness of the phytochemical content, contributing to understanding the potentially active constituents against the H5N1 virus. The findings from docking simulations reveal that specific flavonoid di-glycosides have shown excellent affinity toward essential proteins in the survival and replication of the influenza virus. Notably, hesperidin demonstrated superior binding affinity towards three critical viral proteins, with docking scores approaching or exceeding those of native ligands, establishing a strong scientific basis for the extracts' antiviral capabilities. The study concludes with a practical suggestion to use prepared crude methanol extracts of both plants as an antiviral agent. This recommendation is backed by the extensive research and findings presented, making a compelling case for the natural extracts' therapeutic potential.

The methodology and strengths highlighted in this study poise it as a significant contribution to the field of antiviral research, especially concerning natural products and their nano formulations against influenza viruses.

4. Conclusion

The existence of bioactive combinations such phenolic acids and flavonoids may be the explanation for the antiviral activity of the crude methanol extracts of CML, LAL, and LAF as well as their nano-formulation. Hesperidin, kaempferol-3-*O*-rutinoside and kaempferol-7-neohesperidoside were the most active compounds subjected to docking simulation against five key proteins in survival and replication of influenza virus. So, flavonoid di-glycosides have shown outstanding affinity toward the five investigated proteins and achieved docking scores which approached or even exceeded that achieved by the native ligands. We propose using prepared

crude methanol extracts from both plants as an antiviral agent. We advise studying the activity of *L. acidissima* fruits, leaves, and *C. medica* leaves on other viruses which affect respiratory tract for both birds and humans like MERSA and Corona strains. Potential limitations might include: The study focuses solely on the avian influenza H5N1 virus. This specificity limits the applicability of findings to a broader spectrum of viral pathogens. The research is conducted *in vitro* (or possibly using molecular docking simulations), while valuable, does not account for the complex interactions and metabolism that occur in living organisms. Consequently, the effectiveness of the extracts and nano formulations in animals or humans remains speculative until further in vivo studies are conducted. While molecular docking provides valuable insights into potential interactions between compounds and proteins, it does not fully capture the dynamic nature of these interactions in a live biological context. Docking simulations are theoretical and need validation through empirical experiments. The study relies on extracts from **Citrus medica** and **Limonia acidissima**, plants which could have significant phytochemical variability depending on factors like geography, climate, harvesting time, and processing methods. This variability can affect the reproducibility and consistency of the antiviral effects observed.

While nano formulations (ZnONPs) showcased potent antiviral effects, nanoparticles' behavior in biological systems can be unpredictable. Their long-term stability, toxicity, and interactions with biological molecules and cells need comprehensive exploration. The effectiveness of extracts and nanoparticles at a specific concentration (160 μg) is mentioned, but the study doesn't elaborate on the performance under varied conditions (different concentrations, time points, etc.)., which is necessary for determining the optimal therapeutic window and safety margins.

Understanding the safety profile is critical for any potential therapeutic agent before proceeding to clinical trials. The assessment of the toxicity or side effects of the extracts and nanoparticles not mentioned here it's a point for further investigation.

Compliance with ethical standards

No possible conflicts of interest; Research involving no human participants and/or animals.

Availability of data and material

yes, data included in article/supp. material/referenced in article.

Funding

No funding was received.

Statements & declarations

The authors certify that they did not accept any grants, funding, or other forms of assistance in order to prepare this research.

CRediT authorship contribution statement

Abeer M. El Sayed: Writing – review & editing, Writing – original draft, Supervision, Investigation. **Eman A.W. El-Abd:** Writing – review & editing, Writing – original draft, Methodology. **Ahmed H. Afifi:** Writing – original draft, Methodology. **Fatma A. Hashim:** Writing – original draft, Supervision. **Omnia Kutkat:** Writing – original draft, Methodology, Investigation. **Mohamed A. Ali:** Writing – original draft, Methodology, Investigation. **Mohamed A. El Raey:** Writing – original draft, Methodology, Formal analysis. **Seham S. El Hawary:** Writing – review & editing, Supervision.

Declaration of competing interest

The authors declare that they have no known competing financial interests or personal relationships that could have appeared to influence the work reported in this paper.

Appendix A. Supplementary data

Supplementary data to this article can be found online at https://doi.org/10.1016/j.heliyon.2024.e32335.

References

[1] R. Sood, D. Swarup, S. Bhatia, D.D. Kulkarni, S. Day, M. Saini, S.C. Dubey, Antiviral activity of crude extracts of Eugenia jambolana Lam. against highly pathogenic avian influenza (H5N1) virus, Indian J. Exp. Biol. 50 (2012) 179–186.

[2] S. Ben-Shabat, L. Yarmolinsky, D. Porat, A. Dahan, Antiviral effect of phytochemicals from medicinal plants: applications and drug delivery strategies, Drug Deliv. Transl. Res. 10 (2) (2020) 354–367, https://doi.org/10.1007/s13346-019-00691-6.

[3] S.S. El Hawary, F.A. Hashim, N.A. Ibrahim, A.A.E.M. Matloub, A.M. ElSayed, M.A. Farid, H.M.A.H. Shata, O. Kutkat, E.A.W. El-Abd, M.A. Ali, Comparative study of chemical compositions, antimicrobial and antiviral activities of essential oils for citrus medica var. sarcodactylis Swingle fruits and leaves along with limonia acidissima L. Leaves. Egypt, J. Chem. 65 (8) (2021) 263–270, https://doi.org/10.21608/EJCHEM.2021.108413.4958.

[4] O. Theanphong, T. Songsak, M. Vanish, Chemical composition and antimicrobial activity of the essestial oil from citrus medica L. Var. sarcodactylis (sieber) Swingle leaf, Mahidol University, J. Pharm. Sci 35 (1–4) (2008) 57–61.

[5] H.N. Murthy, D. Dalawai, Bioactive compounds of wood apple (limonia acidissima L.), in: Book: Bioactive Compounds in Underutilized Fruits and Nuts, 2020, pp. 543–569.

[6] C. Pande, G. Tewaria, C. Singha, S. Singha, R.C. Padalia, Chemical composition of the essential oil of Feronia elephantum Correa, Nat. Prod. Res. 24 (19) (2010) 1807–1810.

[7] G.K. Naidu, B. Sujatha, K.C.S. Naidu, In vitro antibacterial activity analysis of leaves of limonia acidissima, Not. Sci. Biol. 6 (2) (2014) 155–157.

[8] S. Suriyaprom, P. Mosoni, S. Leroy, T. Kaewkod, M. Desvaux, Y. Tragoolpua, Antioxidants of fruit extracts as antimicrobial agents against pathogenic bacteria, Antioxidants 11 (2022) 602, https://doi.org/10.3390/antiox11030602.

[9] M. Deli, E.B. Ndjantou, J.T. Ngatchic Metsagang, J. Petit, N. Njintang Yanou, J. Scher, Successive grinding and sieving as a new tool to fractionate polyphenols and antioxidants of plants powders: application to Boscia senega-lensis seeds, Dichrostachys glomerata fruits, and Hibiscus sabdariffa calyx powders, Food Sci. Nutr. 7 (5) (2019) 1795–1806, https://doi.org/10.1002/fsn3.1022.

[10] F.G. Hayden, K.M. Cote, R.G. Douglas, Plaque inhibition assay for drug susceptibility testing of influenza viruses, Antimicrob. Agents Chemother. 17 (1980) 865–870.

[11] T. Mosmann, Rapid colorimetric assays for cellular growth and survival: application to proliferation and cytotoxicity assays, J. Immunol. Methods (1983) 6555–6563.

[12] L-o. Vajrabhaya, S. Korsuwannawong, Cytotoxicity evaluation of a Thai herb using tetrazolium (MTT) and sulforhodamine B (SRB) assays, Journal of Analytical Science and Technology 9 (2018) 15.

[13] A. Kandeil, A. Mostafa, O. Kutkat, Y. Moatasim, A.A. Al-Karmalawy, A.A. Rashad, A.E. Kayed, A.E. Kayed, R. El-Shesheny, G. Kayali, M. Ali, ABioactive polyphenolic compounds showing strong antiviral activities against severe acute respiratory syndrome coronavirus 2, Pathogens 10 (2021) 758.

[14] T. Zhang, D. Wan, Y. Li, S. Wang, X. Zhou, F. Sefidkon, X. UPLC-MS Analysis Yang, Quantification of Compounds, and Comparison of Bioactivity of Methanol Extract and Its Fractions from Qiai (Artemisia argyi Lévl. et Van.), Molecules 28 (5) (2023) 2022, https://doi.org/10.3390/molecules28052022.

[15] G.H. Attia, H.S. Alyami, M.A.A. Orabi, A.H. Gaara, M.A. El Raey, Antimicrobial activity of silver and zinc nanoparticles mediated by eggplant green Calyx, Int. J. Pharmacol. 16 (2020) 236–243.

[16] M.A. Almessiere, Y. Slimani, A.V. Thurkanov, A. Baykal, Structural and morphological characterization of nanomaterials, in: A. Thakur, P. Thakur, S.P. Khurana (Eds.), Synthesis and Applications of Nanoparticles, Springer, Singapore, 2022, https://doi.org/10.1007/978-981-16-6819-7_6.

[17] O. Trott, J.O. Arthur, AutoDock Vina: improving the speed and accuracy of docking with a new scoring function, efficient optimization, and multithreading, J. Comput. Chem. 31 (2) (2010) 455–461.

[18] K. Alagarasu, P. Patil, M. Kaushik, D. Chowdhury, R.K. Joshi, H.V. Hegde, M.B. Kakade, S.L. Hoti, S. Cherian, D. Parashar, In vitro antiviral activity of potential medicinal plant extracts against Dengue and Chikungunya viruses, Front. Cell. Infect. Microbiol. 7 (12) (2022) 866452. https://doi10.3389/fcimb.2022.866452.

[19] S.S. El-Hawary, M.Y. Issa, H.S. Ebrahim, A.F. Mohammed, A.M. Hayallah, E.M. Abd El-Kadder, A.M. Sayed, U.R. Abdelmohsen, Potential of (Citrus nobilis Lour × Citrus deliciosa Tenora) metabolites on COVID-19 virus main protease supported by in silico analysis, Nat. Prod. Res. 36 (11) (2022) 2843–2847.

[20] B. Sornpet, T. Potha, Y. Tragoolpua, K. Pringproa, Antiviral activity of five Asian medicinal pant crude extracts against highly pathogenic H5N1 avian influenza virus, Asian Pac. J. Trop. Med. 10 (9) (2017) 871–876, https://doi.org/10.1016/j.apjtm.2017.08.010.

[21] F. Alam, K. Mohammadin, Z. Shafique, S.T. Amjad, M.H.H.B. Asad, Citrus flavonoids as potential therapeutic agents: a review, Phytother Res. 36 (4) (2022) 1417–1441. https://doi10.1002/ptr.7261.

[22] V.L. Sanches, T.A. Cunha, J. Viganó, L.M. Mesquita, L.H. Faccioli, M.C. Breitkreitz, M.A. Rostagno, Comprehensive analysis of phenolics compounds in citrus fruits peels by UPLC-PDA and UPLC-Q/TOF MS using a fused-core column, Food Chem. X 14 (2022) 100262, https://doi.org/10.1016/j.fochx.2022.100262.

[23] X. Wu, B. Xie, X. Huang, H. Wu, Y. Huo, X. Zhou, Rapid analysis compositions of processed citrus medica L. Var. sarcodactylis Swingle by UPLC-Q-TOF MS, J. Chin. Mass Spectrom. Soc. 42 (3) (2021) 207–217.

[24] M.A. Farag, D.M. Rasheed, M. Kropf, A.G. Heiss, Metabolite profiling in Trigonella seeds via UPLC-MS and GC-MS analyzed using multivariate data analyses, Anal. Bioanal. Chem. 408 (28) (2016) 8065–8078, https://doi.org/10.1007/s00216-016-9910-4.

[25] M.S. Soares, D.F. da Silva, J.C. Amaral, M.M. da Silva, M.R. Forim, E.R. Filho, M.F. da Silva, J.B. Fernandes, M.A. Machado, A.A. de Souza, C.H.G. Martins, Rapid differentiation of graft Citrus sinensis with and without Xylella fastidiosa infection by mass spectrometry, Rapid Commun. Mass Spectrom. 34 (S3) (2020).

[26] M.A. El-Sayed, A.A. Al-Gendy, D.I. Hamdan, El-Shazly, A.M. Phytoconstituents, LC-ESI-MS profile, antioxidant and antimicrobial activities of citrus x limon L. Burm. F. Cultivar variegated pink lemon, J. Pharm. Sci. Res. 9 (4) (2017) 375–391.

[27] Y. Zeng, S. Li, X. Wang, T. Gong, X. Sun, Z. Zhang, Validated LC-MS/MS method for the determination of scopoletin in rat plasma and its application to pharmacokinetic studies, Molecules 20 (2015) 18988–19001.

[28] E.J. Rupa, L. Arunkumar, Y. Han, J.P. Kang, J.C. Ahn, S.K. Jung, M. Kim, J.Y. Kim, D.C. Yang, G.J. Lee, Dendropanax morbifera extract-mediated ZnO nanoparticles loaded with indole-3-carbinol for enhancement of anticancer efficacy in the A549 human lung carcinoma cell line, Materials 13 (14) (2020) 3197, https://doi.org/10.3390/ma13143197.

[29] S.M. Niknam, I. Escudero, J.M. Benito, Formulation and preparation of water-in-oil-in-water emulsions Loaded with a phenolic-rich inner aqueous phase by application of high energy emulsification methods, Foods 9 (10) (2020) 1411, https://doi.org/10.3390/foods9101411.

[30] K. Sahiro, Y. Kawato, K. Koike, T. Sano, T. Nakai, M. Sadakane, Preyssler-type phosphotungstate is a new family of negative-staining reagents for the TEM observation of viruses, Sci. Rep. 12 (1) (2022) 7554, https://doi.org/10.1038/s41598-022-11405-3.

[31] F. Xu, Y. Shi, B. Li, C. Liu, Y. Zhang, J. Zhong, Characterization, stability and antioxidant activity of vanilla nano-emulsion and its complex essential oil, Foods 13 (2024) 801, https://doi.org/10.3390/foods13050801.

[32] T.B. Schreiner, A. Santamaria-Echart, A. Ribeiro, A.M. Peres, M.M. Dias, S.P. Pinho, F.M. Barreiro, Formulation and optimization of nanoemulsions using the natural surfactant saponin from Quillaja bark, Molecules 25 (7) (2020) 1538.

[33] P.B. Chouke, A.K. Potbhare, K.M. Dadure, A.J. Mungole, N.S. Meshram, R. Chaudhary, A.R. Rai, R.G. Chaudhary, An antibacterial activity of Bauhinia racemosa assisted ZnO nanoparticles during lunar eclipse and docking assay, Mater. Today: Proc. 29 (2020) 815–821.

[34] M.M. Melk, S.S. El-Hawary, F.R. Melek, D.O. Saleh, O.M. Ali, M.A. El Raey, N.M. Selim, Antiviral activity of zinc oxide nanoparticles mediated by Plumbago indica L. Extract against herpes simplex virus type 1 (HSV-1), Int. J. Nanomed. 16 (2021) 8221–8233.

[35] V. Srinivasan, H. Brognaro, P.R. Prabhu, et al., Antiviral activity of natural phenolic compounds in complex at an allosteric site of SARS-CoV-2 papain-like protease, Commun. Biol. 5 (2022) 805, https://doi.org/10.1038/s42003-022-03737-7.

[36] G.H. Attia, Y.S. Moemen, M. Youns, A.M. Ibrahim, R. Abdou, M.A. El Raey, Antiviral zinc oxide nanoparticles mediated by hesperidin and in silico comparison study between antiviral phenolics as anti-SARS-CoV-2, Colloids and surfaces. B, Biointerfaces 203 (2021) 111724, https://doi.org/10.1016/j.colsurfb.2021.111724.

[37] A. Chaudhary, N. Kumar, R. Kumar, R.K. Salar, Antimicrobial activity of zinc oxide nanoparticles synthesized from Aloe vera peel extract, SN Appl. Sci. 1 (2019) 136, https://doi.org/10.1007/s42452-018-0144-2.

[38] E.M. Abd Elghani, A.M. El Sayed, M.A. Emam, A.-M. Abdulaziz, S.H. Tadros, F.M. Soliman, F.S. Youssef, Seasonal metabolic profiling of Valencia orange leaf essential oil using GC coupled with chemometrics, nano-formulation, and insecticidal evaluation: in vivo and in silico, RSC Adv. 13 (3) (2023) 1659–1671, https://doi.org/10.1039/D2RA06273A.